

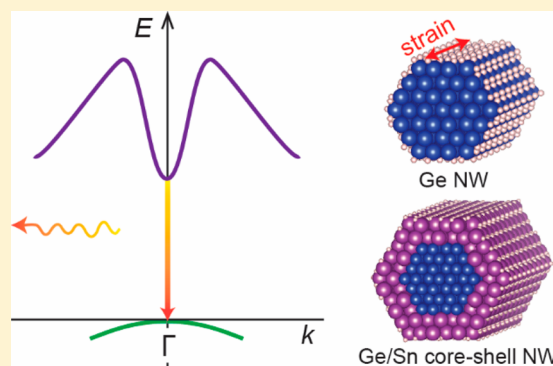
Design of Dipole-Allowed Direct Band Gaps in Ge/Sn Core–Shell Nanowires

Elisabeth Pratidhina, Sunghyun Kim, and K. J. Chang*

Department of Physics, Korea Advanced Institute of Science and Technology, Daejeon 34141, Republic of Korea

 Supporting Information

ABSTRACT: Owing to the indirect band gap nature, Ge exhibits poor optical properties, limiting its usage for optical devices. However, since the direct band gap of Ge is only higher by 0.14 eV than the indirect band gap, band gap engineering has drawn much attention to realize the direct band gap. Here, we report a strategy to design the direct band gap in Ge/Sn core–shell nanowires (NWs), based on first-principles calculations. For [111]-oriented NWs, we show that the direct band gaps can be tuned by controlling the diameter and the core–shell ratio. We find that the intrinsic strain induced by the lattice mismatch between Ge and Sn drives an indirect-to-direct band gap transition. Even for Ge/Sn core–shell NWs with intrinsically indirect band gaps, the direct band gaps can be achieved by applying an external tensile strain lower than the critical values for pure Ge NWs and bulk Ge. The optical transitions of the direct band gaps are all dipole-allowed, suggesting that [111]-oriented Ge/Sn core–shell NWs are promising for applications as light emitters.



1. INTRODUCTION

Semiconductor nanowires have attracted much attention because they exhibit the electrical, optical, and magnetic properties that are different from those of their bulk counterparts due to the quantum confinement effect and the large surface-to-volume ratio.^{1,2} In particular, germanium nanowires (Ge NWs) have been extensively studied because Ge offers the high hole mobility.^{3,4} A variety of potential applications using Ge NWs have been reported, such as field-effect transistor,^{5,6} photodetector,⁷ photoresistor,⁸ Li-ion battery anode,⁹ ultraviolet dosimetry,¹⁰ and spintronic device.¹¹ Moreover, Ge is considered as a potential light source in photonic devices compatible with the current Si technology.^{12–14} However, because large-sized Ge NWs and bulk Ge have indirect band gaps,^{15,16} electron–hole pair recombination can only take place with phonon assistance.

Despite the indirect band gap nature, Ge has the direct band gap that only differs by 0.14 eV from the indirect band gap, while the direct band gap is higher by about 2.3 eV than the indirect band gap in Si.¹⁴ The small difference between the indirect and direct band gaps promotes extensive studies on the band structure engineering of Ge, such as through nanostructuring,^{17,18} strain introduction,^{19–23} and alloying with other group-IV elements.^{24–29} Zone-folding and quantum confinement effects can induce direct band gaps for Ge NWs without strain, which are oriented along the [100] and [110] directions.^{15,16} However, their optical transitions at the threshold energy are not improved due to the indirect gap nature of bulk Ge. Previous theoretical studies reported that strain can reduce the difference between the indirect and the

direct band gaps.^{19–23} In particular, biaxial tensile strain works more effectively than uniaxial strain in deriving the indirect-to-direct gap transition. In the case of uniaxial strain, the critical strain was shown to be generally lower along the [111] direction, while its theoretically predicted values range from 3.7% to 5.7%.^{20–23} Experimentally, the effect of biaxial tensile strain was mostly studied for bulk Ge, with the induced strains up to 2.33%.^{30–36} On the other hand, 5.7% uniaxial tensile strain along the [100] axis was achieved in suspended Ge wires on a Si substrate.³⁷ For [111]-oriented Ge NWs, relatively low uniaxial strains were induced, such as 1.48% uniaxial strain by using silicon nitride stressor layers and 2.5% uniaxial strain by using a micromechanical 3-point stress module.^{38,39} Recently, it has been reported that GeSn alloy with the Sn content of about 12.6% has a direct band gap of 0.55 eV, permitting the demonstration of lasing.²⁹ Although the direct band gap can be achieved by increasing the Sn concentration in GeSn alloys, the band gap is much reduced because Sn has zero gap. On the other hand, Ge NWs take advantage of the quantum confinement effect which enhances the band gap size. Since introducing Sn layers in the shell part of Ge NWs can induce intrinsic tensile strain due to the large lattice mismatch between Sn and Ge ($a_{\text{Ge}} = 5.65 \text{ \AA}$, $a_{\text{Sn}} = 6.48 \text{ \AA}$),⁴⁰ it may overcome the difficulty of accessing large strains during a microfabrication process. Therefore, based on Ge/Sn core–shell structures, one

Received: August 31, 2016

Revised: November 17, 2016

Published: November 18, 2016

may achieve tunable direct band gaps around 1 eV suitable for optical applications.

In this work, we perform first-principles density functional calculations to investigate the electronic and optical properties of Ge/Sn core–shell nanowires oriented along the [111] direction. We propose that the band gaps can be tuned by controlling the wire diameter and the ratio of the Ge core and the Sn shell. We find that the intrinsic strain induced by the lattice mismatch between Ge and Sn drives an indirect-to-direct band gap transition. For Ge/Sn core–shell NWs with intrinsically indirect band gaps, we show that an external tensile strain along the [111] direction can trigger an indirect-to-direct band gap transition; however, the critical strain is significantly reduced, as compared to pure Ge NWs with the same core sizes. We examine the matrix element of direct optical transition and find that all the direct band gaps are dipole-allowed, suggesting that our proposed NWs can serve as an efficient light emitter.

2. CALCULATION METHOD

Our first-principles calculations were performed by using the local density approximation (LDA)^{41,42} for the exchange–correlation potential within the density functional theory framework and the projector augmented wave (PAW) pseudopotentials,^{43,44} as implemented in the VASP code.^{45,46} The wave functions were expanded in plane waves up to a kinetic energy cutoff of 250 eV, and a set of k -points along the wire axis was generated by using the $1 \times 1 \times 8$ Monkhorst–Pack mesh for Brillouin zone (BZ) integration.⁴⁷ Nanowire structures were modeled by including a vacuum region in the supercell geometry, in which adjacent wires were separated by about 10 Å, ensuring for prohibiting wire–wire interactions, and the wire surfaces were passivated with hydrogen. Both the lattice parameters and the ionic coordinates were fully relaxed until the residual forces were less than 0.04 eV/Å. For optimized geometries, the nature of the band gaps (direct vs indirect) was examined by using a dense k -point mesh. Since the band gaps are underestimated by the LDA, we additionally carried out the hybrid functional calculations to confirm the band gap nature for selected nanowires, in which the HSE06 functional of Heyd, Scuseria, and Ernzerhof^{48,49} was used, with the screening parameter of $\omega = 0.207 \text{ \AA}^{-1}$ and the mixing parameter of $\alpha = 0.25$.

3. RESULTS AND DISCUSSION

Bulk Ge has an indirect band gap with the valence band maximum (VBM) and conduction band minimum (CBM) states located at the Γ_b and L_b points, respectively, as illustrated in Figure 1a (henceforth, the subscript b is referred to as the k -points in the bulk BZ). The 4-fold-degenerate CBM states split into a nondegenerate $\epsilon_c(L_b)$ state and 3-fold-degenerate $\epsilon_c(\Gamma_b)$ states under uniaxial strain along the [111] direction. As strain increases, $\epsilon_c(L_b)$ moves up, whereas $\epsilon_c(\Gamma_b)$ moves down with respect to the VBM. On the other hand, the CBM energy at Γ_b decreases faster than the $\epsilon_c(L_b)$ states under the strain. In the absence of strain, experimentally, the difference (Δ) between the conduction band energies at the Γ_b and L_b points is 0.141 eV at room temperature (RT) and 0.154 eV at 1.5 K.^{14,23} For these measured values for Δ , we performed the HSE06 calculations with including the effects of normal compression and internal strain. We find that the critical strains required for the indirect-to-direct band gap transition are 3.8% and 4.1% at

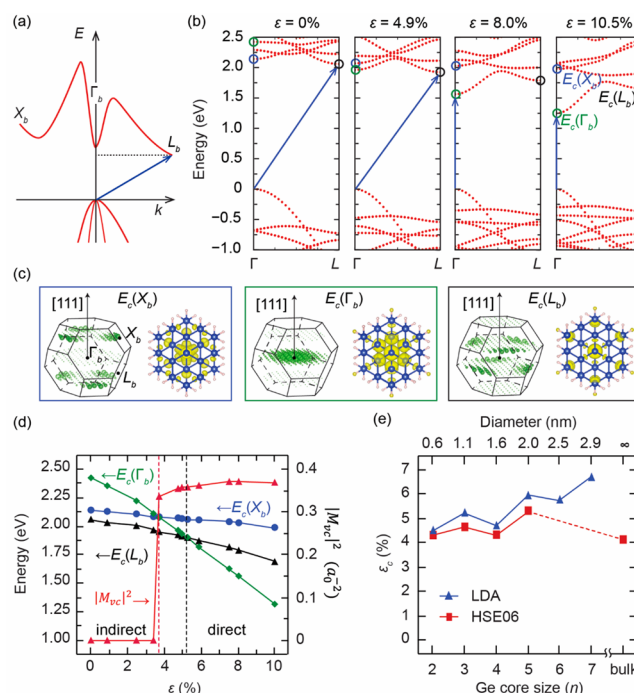


Figure 1. (a) A schematic band diagram of bulk Ge and (b) the LDA band structures of the [111]-oriented Ge₃ NW with the diameter of 10.86 Å under various uniaxial strains (ϵ) along the axial direction. Green, blue, and black circles indicate the conduction band states of Ge NW, $E_c(\Gamma_b)$, $E_c(X_b)$, and $E_c(L_b)$, respectively. (c) The charge distributions for the $E_c(\Gamma_b)$, $E_c(X_b)$, and $E_c(L_b)$ states and their orbital characteristics which represent the degree of contributions from the Γ_b , X_b , and L_b points in the bulk BZ. (d) The variations of $E_c(\Gamma_b)$, $E_c(L_b)$, and $E_c(X_b)$ states and the square of the dipole matrix element of the direct transition at the Γ point under uniaxial strain along the wire axis. Red and black vertical dashed lines represent the strains where the $E_c(\Gamma_b)$ state crosses with the $E_c(X_b)$ and $E_c(L_b)$ states, respectively. (e) The results of the LDA and HSE06 calculations for the critical strain (ϵ_c) at which an indirect-to-direct band gap transition occurs in pure Ge NWs consisting of n Ge layers and bulk Ge.

RT and 1.5 K, respectively, in good agreement with the previous HSE06²³ and quasiparticle GW calculations.²⁰

The band structure of [111]-oriented Ge NWs can be understood in terms of the zone folding of the bulk BZ along the [111] direction. The L_b point is projected onto the L point on the boundary of the NW BZ, while the Γ_b and X_b points are projected onto the center of the BZ (Γ point). Thus, the CBM and VBM states of [111]-oriented Ge NWs will be located at the L and Γ points, respectively. The LDA band structure of Ge NW with the diameter of 10.86 Å is shown in Figure 1b. The axial lattice constant is slightly shortened, as compared to bulk Ge. Nevertheless, it is clear that Ge NW has an indirect band gap in the absence of strain. By using the band-unfolding method^{50–52} and analyzing the orbital characteristics, we confirm that the VBM and CBM states of Ge NW are derived from the Γ_b and L_b points, respectively. While two lowest conduction band states at the Γ point are folded from the Γ_b and X_b points, the conduction band derived from the Γ_b point is higher than that derived from the X_b point, in contrast to bulk Ge where the X_b point is higher in energy than the Γ_b point. Here, we denote $E_c(\Gamma_b)$, $E_c(L_b)$, and $E_c(X_b)$ for the conduction band states of Ge NW, which are derived from the Γ_b , L_b , and X_b points, respectively (Figure 1c). The variations of $E_c(\Gamma_b)$, $E_c(L_b)$, and $E_c(X_b)$ with uniaxial strain are shown in Figure 1b.

Table 1. Diameters and Band Gaps of Ge_n NWs and Ge_n/Sn_m Core–Shell NWs^a

nanowire	d_{core}	d_{total}	LDA		HSE06		gap
			$E_D(\Gamma)$	$E_{ID}(L)$	$E_D(\Gamma)$	$E_{ID}(L)$	
Ge ₂		6.27	3.48	3.23	4.26	4.03	ID
Ge ₂ /Sn ₁	6.85	12.14	1.91	1.93	2.42	2.51	D
Ge ₂ /Sn ₂	7.01	17.52	1.01	1.24	1.36	1.68	D
Ge ₂ /Sn ₃	6.87	22.73	0.42	0.66			D
Ge ₃		10.86	2.14	2.06	2.88	2.78	ID
Ge ₃ /Sn ₁	11.52	16.74	1.37	1.34	1.88	1.87	ID
Ge ₃ /Sn ₂	11.44	22.26	0.74	0.80			D
Ge ₃ /Sn ₃	11.85	27.74	0.25	0.37			D
Ge ₄		15.50	1.59	1.50	2.27	2.16	ID
Ge ₄ /Sn ₁	16.28	21.44	1.10	1.07			ID
Ge ₄ /Sn ₂	16.34	27.12	0.59	0.64			D
Ge ₄ /Sn ₃	16.38	32.48	0.10	0.22			D
Ge ₅		20.10	1.26	1.09	1.92	1.74	ID
Ge ₅ /Sn ₁	20.80	26.05	0.89	0.75			ID
Ge ₅ /Sn ₂	20.89	31.81	0.40	0.36			ID
Ge ₅ /Sn ₃	21.09	37.51	0.05	0.06			D
Ge ₆		24.82	1.09	0.87			ID
Ge ₆ /Sn ₁	25.36	30.81	0.76	0.64			ID

^aHere, d_{core} and d_{total} denote the core and total diameters in units of Å, respectively, and $E_D(\Gamma)$ and $E_{ID}(L)$ represent the direct (D) and indirect (ID) band gaps in units of eV at the Γ and L points, respectively, which were obtained from the LDA and HSE06 calculations.

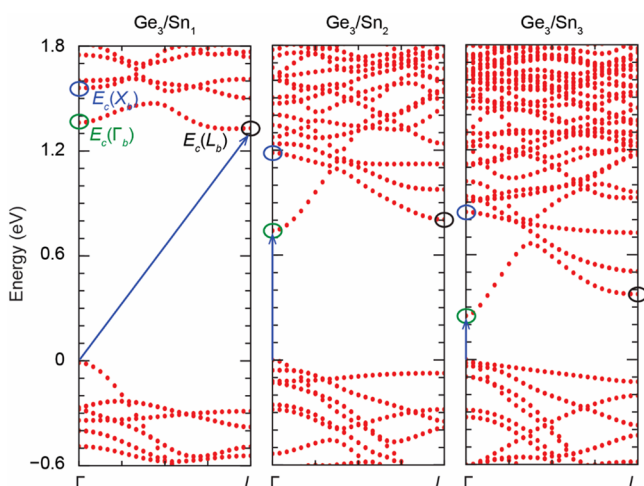


Figure 2. LDA band structures of Ge₃/Sn₁, Ge₃/Sn₂, and Ge₃/Sn₃ core–shell NWs without external strain. Green, blue, and black circles indicate the conduction band states, $E_c(\Gamma_b)$, $E_c(X_b)$, and $E_c(L_b)$, which have the Γ_b , X_b , and L_b -like characters of bulk Ge, respectively.

While all the states tend to decrease with increasing of strain, the downward shift of $E_c(\Gamma_b)$ is more significant (Figure 1d), similar to bulk Ge.^{21,22} The $E_c(\Gamma_b)$ state first crosses with the $E_c(X_b)$ state at 3.7% strain and then with the $E_c(L_b)$ state at 5.2% strain, leading to an indirect-to-direct band gap transition. We examined the optical transition by calculating the square of the dipole matrix element of the direct transition at the Γ point, $|M_{vc}|^2 = |\langle \varphi_c^\Gamma | \hat{p} | \varphi_v^\Gamma \rangle|^2$. We find that $|M_{vc}|^2$ is rapidly enhanced when the band crossing between the $E_c(\Gamma_b)$ and $E_c(X_b)$ states occurs (Figure 1d), indicating that the $E_c(\Gamma_b)$ state allows for the dipole transition.

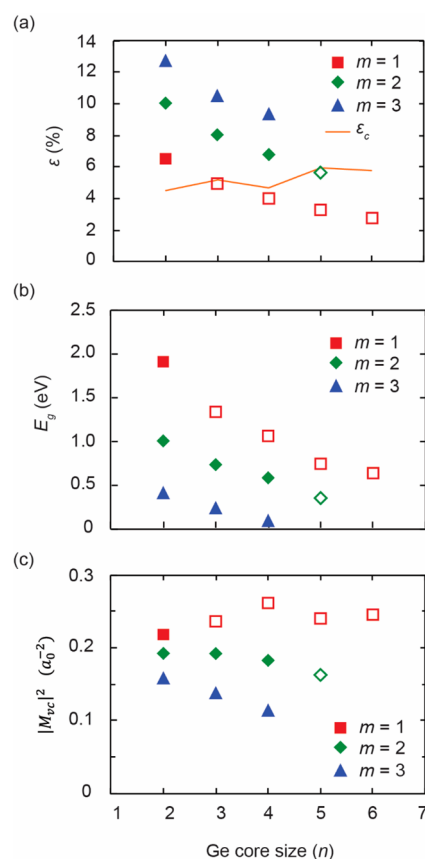


Figure 3. (a) The intrinsic tensile strains (ϵ), (b) the LDA band gaps (E_g), and (c) the squares of the dipole matrix elements of the direct transition at the Γ point ($|M_{vc}|^2$) in $[111]$ -oriented Ge_n/Sn_m core–shell NWs with n Ge layers in the core and m Sn layers in the shell. The orange line in (a) represents the critical strains (ϵ_c) for the indirect-to-direct transition in pure Ge NWs with the same Ge cores. Filled and unfilled markers stand for the NW structures with the direct and indirect band gaps, respectively.

Figure 1e shows the critical strain required for the indirect-to-direct band gap transition in $[111]$ -oriented Ge NWs with the diameters of about 6.27–29.01 Å. For diameters up to 20.10 Å, the critical strain obtained from HSE06 are in the range of 4.3–5.3%, close to the LDA results of 4.5–5.9%. For the Ge NW with the diameter of 10.86 Å, the critical strain of about 5.3% was reported,²⁰ in good agreement with our LDA calculations. It is noticeable that the critical strains in Ge NWs are higher than the HSE06 result of 4.1% for bulk Ge. In the nanowire, the energy difference between the $E_c(\Gamma_b)$ and the $E_c(L_b)$ states is larger than that of bulk Ge because the L_b -valley states split by the symmetry breaking. Consequently, a larger tensile strain is required to drive the indirect-to-direct transition.

For bulk Ge, tensile strain along the $[100]$ direction also drives an indirect-to-direct transition.^{22,23} However, for the $[100]$ -oriented Ge NW with the diameter of about 20.81 Å, the indirect-to-direct transition does not take place under uniaxial strain up to 10% (see Figure S1 in the Supporting Information). On the other hand, the $[110]$ -oriented Ge NW with the diameter of about 21.88 Å has a direct band gap even in the absence of strain. However, its optical transition at the threshold energy is not dipole-allowed because the CBM state has the L_b -like character. Moreover, since the VBM state shifts away from the Γ point under uniaxial strain along the $[110]$

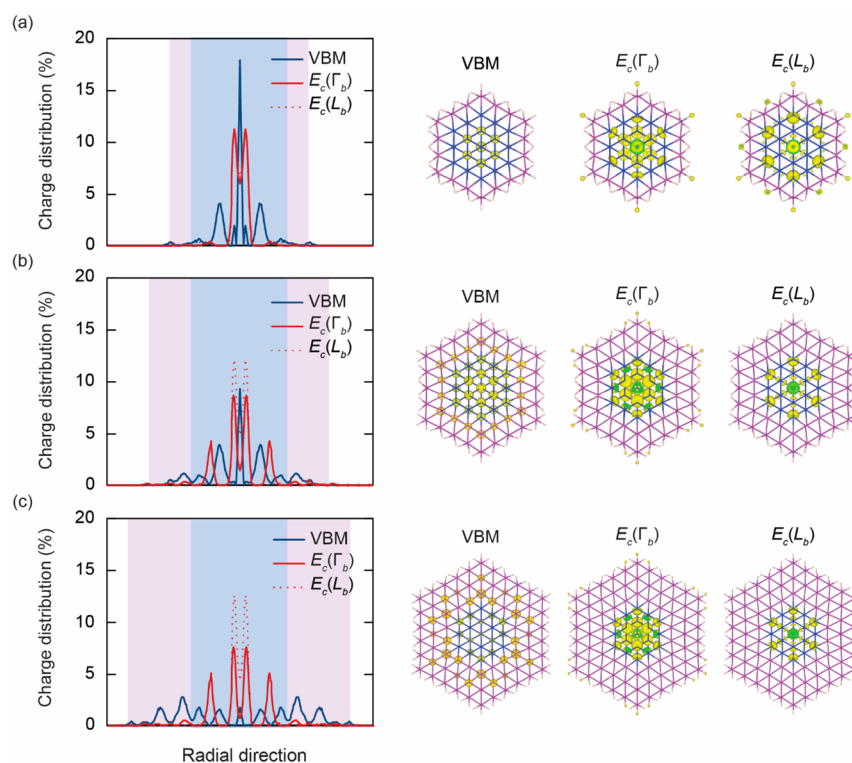


Figure 4. (left) The charge distributions of the valence band maximum (VBM) and the conduction band edge states at the Γ and L points, $E_c(\Gamma_b)$ and $E_c(L_b)$, along the radial direction and (right) their spatial distributions over the wire cross section in (a) Ge_3/Sn_1 , (b) Ge_3/Sn_2 , and (c) Ge_3/Sn_3 core-shell NWs. Blue, purple, and white backgrounds in the left panel correspond to the Ge core, Sn shell, and vacuum regions, respectively.

direction, the band gap changes from direct to indirect (see Figure S2 in the Supporting Information).

We propose a different route to achieve direct band gap nanowires by constructing Ge/Sn core-shell NWs with the radial heterostructure. Since the lattice constant of Sn is larger than that of Ge, the Sn shell induces tensile strain on the Ge core. We considered [111]-oriented Ge_n/Sn_m core-shell NWs, where the Ge core of n layers ($n = 2-6$) is wrapped with the Sn shell of m layers ($m = 1-3$). The nanowire diameters range from 12.14 to 37.51 Å (Table 1). For a given Ge core size, we find a tendency that the indirect band gap turns to the direct band gap as the shell thickness increases. To confirm that, the band structures of Ge_3/Sn_m core-shell NWs are compared with those for tensile-strained Ge_3 NWs with only the Ge core of three layers. While the Ge_3/Sn_1 NW has the indirect band gap of 1.34 eV, the direct band gaps of 0.74 and 0.25 eV occur for the Ge_3/Sn_2 and Ge_3/Sn_3 NWs, respectively (Figure 2). For the Ge_3/Sn_1 , Ge_3/Sn_2 , and Ge_3/Sn_3 NWs, the intrinsic strains are estimated to be 4.9, 8.0, and 10.5%, respectively, when the equilibrium lattice constant of the pure Ge_3 NW is used as a reference. The Ge_3 NW exhibits the same tendency that the indirect band gap decreases as strain increases up to 4.9%, and it turns to the direct band gap for higher strains of 8.0% and 10.5% (Figure 1b). It is verified that Ge/Sn core-shell NWs have direct band gaps when their intrinsic tensile strains are larger than the critical values for Ge NWs with only the Ge cores (Figure 1e and Figure 3a). In addition, we find that the intrinsic tensile strain induced on the Ge core is inversely proportional to the core size, whereas it is proportional to the Sn shell thickness. For Ge/Sn core-shell NWs with large diameters, which cannot be handled within the first-principles LDA calculations, we estimate the intrinsic strain induced on

the Ge core by using a continuum elasticity theory⁵³ (see Figure S3 in the Supporting Information). For small-diameter NWs, we find good agreements between the two different calculations.

The band gap of Ge/Sn core-shell NWs can be tuned by controlling the diameter and the core-to-shell ratio, as shown in Figure 3b. As the Sn shell becomes thicker, the contribution of the Sn orbitals to the band edge states is enhanced, resulting in the reduction of the band gap because Sn has zero band gap.⁵⁴ Moreover, since the thicker Sn shell increases the intrinsic strain on the Ge core, the band gap is also reduced. On the other hand, for a given shell thickness, the band gap increases as the Ge core size decreases due to the stronger quantum confinement effect. For Ge_n/Sn_m core-shell NWs with the diameters of 12.14–37.51 Å ($n = 2-6$ and $m = 1-3$), all the band structures are shown in Figure S4 in the Supporting Information. The direct band gaps calculated by the LDA range from 0.05 to 1.91 eV (Table 1). For selected NWs with the diameters less than 18 Å, the band gaps increase by 27–40% with the hybrid HSE06 functional, exhibiting the largest band gap of 2.42 eV for $n = 2$ and $m = 1$. The variable direct band gaps of about 1 eV will be suitable for applications including optical communications. Experiments have reported the synthesis of Ge NWs with the diameters of about 3 nm.⁵⁵ For the pure Ge_7 NW with the diameter of about 3 nm, the indirect-to-direct transition takes place at about 6.3% strain and the band gap is estimated to be about 1 eV at the critical strain (see Figure S5 in the Supporting Information). According to the continuum elasticity model (see Figure S3 in the Supporting Information), the Sn shell of about 1 nm thickness ($m \sim 4$) is required to induce the intrinsic strain of 6.3% on the Ge_7 core. With including a band gap correction for the pure

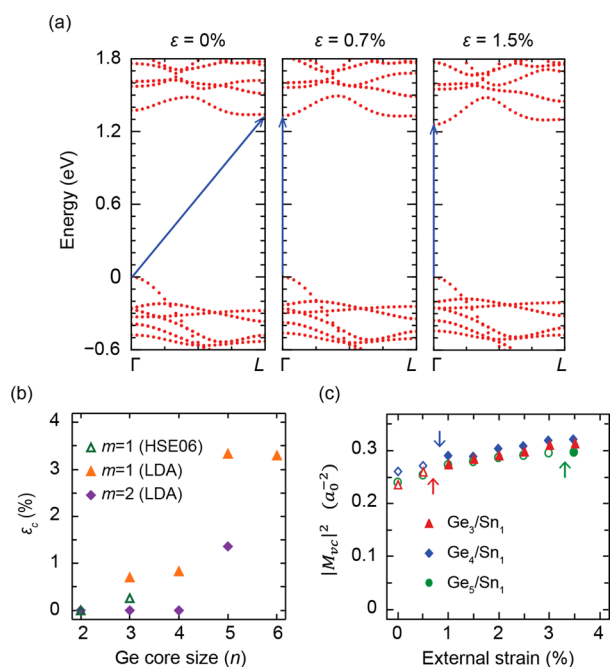


Figure 5. (a) The variation of the LDA band structure of the Ge_3/Sn_1 core-shell NW under external tensile strain (ϵ). The indirect-to-direct band gap transition occurs at 0.7% strain. (b) The external critical strains (ϵ_c) for the indirect-to-direct band gap transition in Ge_n/Sn_1 and Ge_n/Sn_2 core-shell NWs from the LDA and HSE06 calculations. External strain is defined with respect to the equilibrium lattice constants of Ge/Sn core-shell NWs. (c) Squares of dipole matrix element for the direct transition at the Γ point as a function of external strain. Filled and empty symbols in (c) denote the direct and indirect band gaps, respectively, and arrows indicate the critical strains where the indirect-to-direct gap transition occurs.

Ge_7 NW, we expect that the band gaps of Ge_7/Sn_m core-shell NWs with $m = 0-4$ lie in the range of 0.3–1.3 eV (see Table S2 and Figure S6 in the Supporting Information).

The dipole allowedness of the direct transition at the Γ point is examined by calculating the square of the dipole matrix element $|M_{vc}|^2$. For Ge/Sn core-shell NWs with direct band gaps, the squared dipole matrix elements were calculated to be 0.11–0.22 a_0^{-2} in atomic units (Figure 3c), where a_0 is the Bohr radius. These values are much higher than 0.03 a_0^{-2} obtained for a specially designed Si/Ge superstructure,¹⁸ while they are slightly lower than that of GaAs (0.31 a_0^{-2}).⁵⁶ When the core size is fixed, the squared dipole matrix elements tend to decrease as the shell thickness increases. To understand this trend, we examined the charge distributions of the energy states near the band gap for Ge_3/Sn_1 , Ge_3/Sn_2 , and Ge_3/Sn_3 NWs (Figure 4). We find that the $E_c(\Gamma_b^-)$ and $E_c(L_b^-)$ states are mainly distributed over the Ge core, regardless of the shell size. On the other hand, as the Sn shell becomes thicker, the charge distribution of the VBM state extends to the shell region, while the CBM state maintains the localization in the core region. Thus, the overlap between the VBM and CBM states decreases, reducing the optical transition probability. We note that Ge/Sn core-shell NWs with thin Sn shells exhibit the band alignment of type-I, although bulk Sn has the metallic band structure. The type-I band alignment is attributed to the nonzero band gap of the Sn shell, which results from the strong quantum confinement effect, similar to pure Sn NWs (see Table S2 in the Supporting Information).

We investigate the effect of external tensile strain on the indirect-to-direct transition in Ge/Sn core-shell NWs with indirect band gaps. If the Sn shell consists of only one layer, Ge_n/Sn_1 core-shell NWs have intrinsically indirect band gaps for $n \geq 3$ (Table 1). We find that the external critical strain is significantly reduced in Ge/Sn core-shell NWs, compared with pure Ge NWs. For example, the LDA critical strain is estimated to be 0.7% for the Ge_3/Sn_1 core-shell NW (Figure 5a,b), while it is about 5.2% in the pure Ge_3 NW with the same core size (Figure 1e). Moreover, external strain also slightly improves the optical transition in Ge/Sn core-shell NWs, as shown in Figure 5c. When 0.7% tensile strain is applied to the Ge_3/Sn_1 core-shell NW, the square of the dipole matrix element for the direct transition at the Γ point increases from 0.24 to 0.27 a_0^{-2} . Similar strain effects are found for Ge_n/Sn_1 core-shell NWs with $n \geq 4$. However, the critical strain tends to increase as the core size increases, as shown in Figure 5b, while its values are generally lower than those for pure Ge NWs and bulk Ge.

Finally, we discuss the possible synthesis of Ge/Sn core-shell NWs. We compare the formation energy of the Ge_4/Sn_2 core-shell NW with those of GeSn alloy NWs with the same Sn content. We generate five GeSn alloy NWs, in which the Ge and Sn atoms are randomly distributed, whereas the outermost shells are composed of the Sn atoms to avoid the formation of different Ge–H and Sn–H bonds on the wire surface (see Figure S7 in the Supporting Information). We find that the average energy of the GeSn alloy NWs is lower by about 40 meV per Sn atom than that of the core-shell NW. On the other hand, an isolated Sn atom is energetically more favorable near the surface in pure Ge NWs due to the local strain effect. Moreover, the activation enthalpy for the diffusion of Sn in Ge is around 3 eV.⁵⁷ Considering the small energy difference between the core-shell and alloy NWs, we do not rule out the possibility that the Ge/Sn core-shell structure can be synthesized by a controlled epitaxial growth of the Sn shell on the Ge NW, similar to other core-shell or multishell nanowires.⁵⁸ Our results are also supported by recent experiments reported that uniaxial tensile strain can be achieved in Ge/GeSn multishells grown on a one-dimensional Si pillar or cavity, leading to the indirect-to-direct gap transition of Ge.⁵⁹

4. CONCLUSIONS

In conclusion, we have shown that the dipole-allowed direct band gaps can be achieved by wrapping [111]-oriented Ge NWs with Sn layers in the form of core-shell NWs with the radial heterostructure, without applying an external strain. The band gaps can be tuned by controlling the diameter and the core-to-shell ratio. The indirect-to-direct band gap transition is attributed to the intrinsic tensile strain induced by the lattice mismatch between the Ge core and the Sn shell. Due to the band crossing between the bulk Γ_b^- and L_b^- -derived states, the optical transitions of the direct band gaps are all dipole-allowed. For Ge/Sn core-shell NWs with intrinsically indirect band gaps, an external strain can be used to induce the indirect-to-direct transition; however, the critical values are much lower than those for bulk Ge and pure Ge NWs with the same core sizes. The dipole allowedness of the direct band gaps suggests that [111]-oriented Ge/Sn core-shell NWs can serve as potential candidate materials for light emitters.

■ ASSOCIATED CONTENT

Supporting Information

The Supporting Information is available free of charge on the ACS Publications website at DOI: 10.1021/acs.jpcc.6b08779.

The band structures of [100]- and [110]-oriented Ge NWs under uniaxial tensile strain, the detailed modeling of intrinsic strain on large-sized Ge/Sn core-shell NWs, based on the elasticity theory, the band structures of Ge/Sn core-shell NWs with different core sizes and core-to-shell ratios, the variation of the band gap of Ge₇NW with the diameter of ~3 nm under strain, the expected band gaps with gap corrections of Ge/Sn core-shell NWs, and the atomic structures of GeSn alloy NWs (PDF)

■ AUTHOR INFORMATION

Corresponding Author

*E-mail: kjchang@kaist.ac.kr. Phone: 82-42-350-2531. Fax: 82-42-350-2510.

ORCID

K. J. Chang: 0000-0002-5364-8551

Author Contributions

E.P., S.K., and K.J.C. contributed equally to this manuscript. K.J.C. conceived the work and designed the research strategy. E.P. performed theoretical calculations, and E.P. and S.K. did data analysis. All authors discussed the results and co-wrote the manuscript.

Notes

The authors declare no competing financial interest.

■ ACKNOWLEDGMENTS

This work was supported by Samsung Science and Technology Foundation under Grant No. SSTF-BA1401-08.

■ REFERENCES

- (1) Ma, D. D. D.; Lee, C. S.; Au, F. C. K.; Tong, S. Y.; Lee, S. T. Small-Diameter Silicon Nanowire Surfaces. *Science* **2003**, *299*, 1874–1877.
- (2) Zhong, Z.; Wang, D.; Cui, Y.; Bockrath, M. W.; Lieber, C. M. Nanowire Crossbar Arrays as Address Decoders for Integrated Nanosystems. *Science* **2003**, *302*, 1377–1379.
- (3) Pillarisetty, R. Academic and Industry Research Progress in Germanium Nanodevices. *Nature* **2011**, *479*, 324–328.
- (4) Niquet, Y.-M.; Delerue, C. Carrier Mobility in Strained Ge Nanowires. *J. Appl. Phys.* **2012**, *112*, 084301.
- (5) Wang, D.; Wang, Q.; Javey, A.; Tu, R.; Dai, H.; Kim, H.; McIntyre, P. C.; Krishnamohan, T.; Saraswat, K. C. Germanium Nanowire Field-Effect Transistors with SiO₂ and High-κ HfO₂ Gate Dielectrics. *Appl. Phys. Lett.* **2003**, *83*, 2432–2434.
- (6) Greytak, A. B.; Lauhon, L. J.; Gudiksen, M. S.; Lieber, C. M. Growth and Transport Properties of Complementary Germanium Nanowire Field-Effect Transistors. *Appl. Phys. Lett.* **2004**, *84*, 4176–4178.
- (7) Ahn, Y. H.; Park, J. Efficient Visible Light Detection Using Individual Germanium Nanowire Field Effect Transistors. *Appl. Phys. Lett.* **2007**, *91*, 162102.
- (8) Polyakov, B.; Daly, B.; Prikulis, J.; Lissauskas, V.; Vengalis, B.; Morris, M. A.; Holmes, J. D.; Erts, D. High-Density Arrays of Germanium Nanowire Photoresistors. *Adv. Mater.* **2006**, *18*, 1812–1816.
- (9) Chan, C. K.; Zhang, X. F.; Cui, Y. High Capacity Li Ion Battery Anodes Using Ge Nanowires. *Nano Lett.* **2008**, *8*, 307–309.
- (10) Zahedifar, M.; Hosseinmardi, F.; Eshraghi, L.; Ganjipour, B. Synthesis and Thermoluminescence of Boron-Doped Germanium Nanowires. *Radiat. Phys. Chem.* **2011**, *80*, 324–327.

(11) Patibandla, S.; Pramanik, S.; Bandyopadhyay, S.; Tepper, G. C. Spin Relaxation in a Germanium Nanowire. *J. Appl. Phys.* **2006**, *100*, 044303.

(12) Ye, H.; Yu, J. Germanium Epitaxy on Silicon. *Sci. Technol. Adv. Mater.* **2014**, *15*, 024601.

(13) Zhou, Z.; Yin, B.; Michel, J. On-Chip Light Sources for Silicon Photonics. *Light: Sci. Appl.* **2015**, *4*, e358.

(14) Geiger, R.; Zabel, T.; Sigg, H. Group IV Direct Band Gap Photonics: Methods, Challenges, and Opportunities. *Front. Mater.* **2015**, *2*, 52.

(15) Medaboina, D.; Gade, V.; Patil, S. K. R.; Khare, S. V. Effect of Structure, Surface Passivation, and Doping on the Electronic Properties of Ge Nanowires: A First-Principles Study. *Phys. Rev. B: Condens. Matter Mater. Phys.* **2007**, *76*, 205327.

(16) Lee, A. J.; Kim, M.; Lena, C.; Chelikowsky, J. R. Mechanical and Electronic Properties of Strained Ge Nanowires Using *Ab Initio* Real-Space Pseudopotentials. *Phys. Rev. B: Condens. Matter Mater. Phys.* **2012**, *86*, 115331.

(17) Zhang, L.; d'Avezac, M.; Luo, J.-W.; Zunger, A. Genomic Design of Strong Direct-Gap Optical Transition in Si/Ge Core/Multishell Nanowires. *Nano Lett.* **2012**, *12*, 984–991.

(18) d'Avezac, M.; Luo, J.-W.; Chanier, T.; Zunger, A. Genetic-Algorithm Discovery of a Direct-Gap and Optically Allowed Superstructure from Indirect-Gap Si and Ge Semiconductors. *Phys. Rev. Lett.* **2012**, *108*, 027401.

(19) Yang, C. H.; Yu, Z. Y.; Liu, Y. M.; Lu, P. F.; Gao, T.; Li, M.; Manzoor, S. Dependence of Electronic Properties of Germanium on the In-Plane Biaxial Tensile Strains. *Phys. B* **2013**, *427*, 62–67.

(20) Zhang, F.; Crespi, V. H.; Zhang, P. Prediction that Uniaxial Tension along <111> Produces a Direct Band Gap in Germanium. *Phys. Rev. Lett.* **2009**, *102*, 156401.

(21) Hoshina, Y.; Iwasaki, K.; Yamada, A.; Konagai, M. First-Principles Analysis of Indirect-to-Direct Band Gap Transition of Ge under Tensile Strain. *Jpn. J. Appl. Phys.* **2009**, *48*, 04C125.

(22) Liu, L.; Zhang, M.; Hu, L.; Di, Z.; Zhao, S.-J. Effect of Tensile Strain on the Electronic Structure of Ge: A First-Principles Calculation. *J. Appl. Phys.* **2014**, *116*, 113105.

(23) Inaoka, T.; Furukawa, T.; Toma, R.; Yanagisawa, S. Tensile-Strain Effect of Inducing the Indirect-to-Direct Band-Gap Transition and Reducing the Band-Gap Energy of Ge. *J. Appl. Phys.* **2015**, *118*, 105704.

(24) Pandey, R.; Rérat, M.; Causà, M. First-Principles Study of Stability, Band Structure, and Optical Properties of the Ordered Ge_{0.50}Sn_{0.50} Alloy. *Appl. Phys. Lett.* **1999**, *75*, 4127–4129.

(25) Zhang, P.; Crespi, V. H.; Chang, E.; Louie, S. G.; Cohen, M. L. Computational Design of Direct Bandgap Semiconductors that Lattice-Match Silicon. *Nature* **2001**, *409*, 69–71.

(26) Low, K. L.; Yang, Y.; Han, G.; Fan, W.; Yeo, Y.-C. Electronic Band Structure and Effective Mass Parameters of Ge_{1-x}Sn_x Alloys. *J. Appl. Phys.* **2012**, *112*, 103715.

(27) Lee, M.-H.; Liu, P.-L.; Hong, Y.-A.; Chou, Y.-T.; Hong, J.-Y.; Siao, Y.-J. Electronic Band Structures of Ge_{1-x}Sn_x Semiconductors: A First-Principles Density Functional Theory Study. *J. Appl. Phys.* **2013**, *113*, 063517.

(28) von den Driesch, N.; Stange, D.; Wirths, S.; Mussler, G.; Holländer, B.; Ikonik, Z.; Hartmann, J. M.; Stoica, T.; Mantl, S.; Grützmacher, D.; et al. Direct Bandgap Group IV Epitaxy on Si for Laser Applications. *Chem. Mater.* **2015**, *27*, 4693–4702.

(29) Wirths, S.; Geiger, R.; von den Driesch, N.; Mussler, G.; Stoica, T.; Mantl, S.; Ikonik, Z.; Luysberg, M.; Chiussi, S.; Hartmann, J. M.; et al. Lasing in Direct-Bandgap GeSn Alloy Grown on Si. *Nat. Photonics* **2015**, *9*, 88–92.

(30) Sánchez-Pérez, J. R.; Boztug, C.; Chen, F.; Sudradjat, F. F.; Paskiewicz, D. M.; Jacobson, R.; Lagally, M. G.; Paiella, R. Direct-Bandgap Light-Emitting Germanium in Tensilely Strained Nanomembranes. *Proc. Natl. Acad. Sci. U. S. A.* **2011**, *108*, 18893–18898.

(31) Huo, Y.; Lin, H.; Chen, R.; Makarova, M.; Rong, Y.; Li, M.; Kamins, T. I.; Vuckovic, J.; Harris, J. S. Strong Enhancement of Direct

Transition Photoluminescence with Highly Tensile-Strained Ge Grown by Molecular Beam Epitaxy. *Appl. Phys. Lett.* **2011**, *98*, 011111.

(32) Jain, J. R.; Hryciw, A.; Baer, T. M.; Miller, D. A. B.; Brongersma, M. L.; Howe, R. T. A Micromachining-Based Technology for Enhancing Germanium Light Emission via Tensile Strain. *Nat. Photonics* **2012**, *6*, 398–405.

(33) Nam, D.; Sukhdeo, D.; Cheng, S.-L.; Roy, A.; Huang, K. C.-Y.; Brongersma, M.; Nishi, Y.; Saraswat, K. Electroluminescence from Strained Germanium Membranes and Implications for an Efficient Si-Compatible Laser. *Appl. Phys. Lett.* **2012**, *100*, 131112.

(34) Capellini, G.; Kozłowski, G.; Yamamoto, Y.; Lisker, M.; Wenger, C.; Niu, G.; Zaumseil, P.; Tillack, B.; Ghrib, A.; de Kersauson, M.; et al. Strain Analysis in SiN/Ge Microstructures Obtained via Si-Complementary Metal Oxide Semiconductor Compatible Approach. *J. Appl. Phys.* **2013**, *113*, 013513.

(35) Ghrib, A.; El Kurdi, M.; de Kersauson, M.; Prost, M.; Sauvage, S.; Checoury, X.; Beaudoin, G.; Sagnes, I.; Boucaud, P. Tensile-Strained Germanium Microdisks. *Appl. Phys. Lett.* **2013**, *102*, 221112.

(36) El Kurdi, M.; Prost, M.; Ghrib, A.; Sauvage, S.; Checoury, X.; Beaudoin, G.; Sagnes, I.; Picardi, G.; Ossikovski, R.; Boucaud, P. Direct Band Gap Germanium Microdisks Obtained with Silicon Nitride Stressor Layers. *ACS Photonics* **2016**, *3*, 443–448.

(37) Sukhdeo, D. S.; Nam, D.; Kang, J.-H.; Brongersma, M. L.; Saraswat, K. C. Direct Bandgap Germanium-on-Silicon Inferred from 5.7% < 100 > Uniaxial Tensile Strain. *Photonics Res.* **2014**, *2*, A8–A13.

(38) Guilloy, K.; Pauc, N.; Gassenq, A.; Gentile, P.; Tardif, S.; Rieutord, F.; Calvo, V. Tensile Strained Germanium Nanowires Measured by Photocurrent Spectroscopy and X-ray Microdiffraction. *Nano Lett.* **2015**, *15*, 2429–2433.

(39) Greil, J.; Lugstein, A.; Zeiner, C.; Strasser, G.; Bertagnolli, E. Tuning the Electro-optical Properties of Germanium Nanowires by Tensile Strain. *Nano Lett.* **2012**, *12*, 6230–6234.

(40) Haas, P.; Tran, F.; Blaha, P. Calculation of the Lattice Constant of Solids with Semilocal Functionals. *Phys. Rev. B: Condens. Matter Mater. Phys.* **2009**, *79*, 085104.

(41) Ceperley, D. M.; Alder, B. J. Ground State of the Electron Gas by a Stochastic Method. *Phys. Rev. Lett.* **1980**, *45*, 566–569.

(42) Perdew, J. P.; Zunger, A. Self-Interaction Correction to Density-Functional Approximations for Many-Electrons Systems. *Phys. Rev. B: Condens. Matter Mater. Phys.* **1981**, *23*, 5048–5079.

(43) Blöchl, P. E. Projected Augmented-Wave Method. *Phys. Rev. B: Condens. Matter Mater. Phys.* **1994**, *50*, 17953–17979.

(44) Kresse, G.; Joubert, D. From Ultrasoft Pseudopotentials to the Projector Augmented-Wave Method. *Phys. Rev. B: Condens. Matter Mater. Phys.* **1999**, *59*, 1758–1775.

(45) Kresse, G.; Furthmüller, J. Efficient Iterative Schemes for *Ab Initio* Total-Energy Calculations Using a Plane-Wave Basis Set. *Phys. Rev. B: Condens. Matter Mater. Phys.* **1996**, *54*, 11169–11186.

(46) Kresse, G.; Furthmüller, J. Efficiency of *Ab-Initio* Total Energy Calculations for Metals and Semiconductors Using a Plane-Wave Basis Set. *Comput. Mater. Sci.* **1996**, *6*, 15–50.

(47) Monkhorst, H. J.; Pack, J. D. Special Points for Brillouin-Zone Integration. *Phys. Rev. B* **1976**, *13*, 5188–5192.

(48) Heyd, J.; Scuseria, G. E.; Ernzerhof, M. Hybrid Functionals Based on a Screened Coulomb Potential. *J. Chem. Phys.* **2003**, *118*, 8207–8215.

(49) Heyd, J.; Scuseria, G. E.; Ernzerhof, M. Erratum: “Hybrid Functionals Based on a Screened Coulomb Potential” [*J. Chem. Phys.* **118**, 8207 (2003)]. *J. Chem. Phys.* **2006**, *124*, 219906.

(50) Popescu, V.; Zunger, A. Extracting *E* versus *k* Effective Band Structure from Supercell Calculations on Alloys and Impurities. *Phys. Rev. B: Condens. Matter Mater. Phys.* **2012**, *85*, 085201.

(51) Allen, P. B.; Berlijn, T.; Casavant, D. A.; Soler, J. M. Recovering Hidden Bloch Character: Unfolding Electrons, Phonons, and Slabs. *Phys. Rev. B: Condens. Matter Mater. Phys.* **2013**, *87*, 085322.

(52) Tomić, M.; Jeschke, H. O.; Valenti, R. Unfolding of Electronic Structure through Induced Representations of Space Groups: Application to Fe-Based Superconductors. *Phys. Rev. B: Condens. Matter Mater. Phys.* **2014**, *90*, 195121.

(53) Raychaudhuri, S.; Yu, E. T. Calculation of Critical Dimensions for Wurtzite and Cubic Zinc Blende Coaxial Nanowire Heterostructures. *J. Vac. Sci. Technol. B* **2006**, *24*, 2053–2059.

(54) Ansari, L.; Fagas, G.; Colinge, J.-P.; Greer, J. C. A Proposed Confinement Modulated Gap Nanowire Transistor Based on a Metal (Tin). *Nano Lett.* **2012**, *12*, 2222–2227.

(55) Simanullang, M.; Usami, K.; Kodera, T.; Uchida, K.; Oda, S. Germanium Nanowires with 3-nm-Diameter Prepared by Low Temperature Vapour-Liquid-Solid Chemical Vapour Deposition. *J. Nanosci. Nanotechnol.* **2011**, *11*, 8163–8168.

(56) Ossicini, S.; Pavesi, L.; Priolo, F. *Light Emitting Silicon for Microphotonics*; Springer: Berlin, 2003.

(57) Chroneos, A.; Bracht, H.; Grimes, R. W.; Uberuaga, B. P. Vacancy-Mediated Dopant Diffusion Activation Enthalpies for Germanium. *Appl. Phys. Lett.* **2008**, *92*, 172103.

(58) Lauhon, L. J.; Gudixsen, M. S.; Wang, D.; Lieber, C. M. Epitaxial Core-Shell and Core-Multishell Nanowire Heterostructures. *Nature* **2002**, *420*, 57–61.

(59) Huang, Z.-M.; Huang, W.-Q.; Liu, S.-R.; Dong, T.-G.; Wang, G.; Wu, X.-K.; Qin, C.-J. Emission of Direct-Gap Band in Germanium with Ge-GeSn Layers on One-Dimensional Structure. *Sci. Rep.* **2016**, *6*, 24802.